

Non-perturbative determination of the QCD Equation of State up to the electroweak scale

Michele Pepe^{a,*}

^a*INFN, Sezione di Milano-Bicocca, Piazza della Scienza 3, I-20126 Milano, Italy*

E-mail: michele.pepe@mib.infn.it

The QCD Equation of State with $N_f = 3$ massless quark flavours is determined non-perturbatively over a broad range of temperatures, extending from the electroweak scale down to 3 GeV, and smoothly connecting to the low-temperature regime. The comparison with perturbative predictions shows that, even at temperatures approaching the electroweak scale, the Equation of State can be accurately described only by adding terms beyond the known perturbative series, including non-perturbative contributions. The strategy that allows this investigation in the previously unexplored high-temperature regime combines shifted boundary conditions with a determination of the lines of constant physics based on the running of a non-perturbatively defined renormalized coupling. This methodology is general and can be applied to QCD with four or five massive quark flavours.

*The 42nd International Symposium on Lattice Field Theory (LATTICE2025)
2-8 November 2025
Tata Institute of Fundamental Research, Mumbai, India*

*Speaker

1. Introduction

The Equation of State (EoS) of Quantum Chromodynamics (QCD) characterizes the thermodynamic properties of strongly interacting matter in thermal equilibrium. Its determination is a cornerstone of modern physics, bridging the gap between the microscopic dynamics of quarks and gluons and the macroscopic cosmological evolution. While the EoS is a crucial input for hydrodynamic models of the quark-gluon plasma generated in heavy-ion collisions at the hadronic scale ($T \sim 150$ MeV), its relevance extends far beyond this regime. In the early Universe, as the temperature decreased from the electroweak scale ($T \sim 100$ GeV) toward the QCD crossover, the QCD EoS governed the expansion rate and the evolution of the effective number of relativistic degrees of freedom, with direct implications for the spectrum of primordial gravitational waves [1].

Despite its critical importance, first-principles lattice determinations of the QCD EoS have so far been limited up to temperatures of about 1 GeV for theories with $N_f = 2+1$ [2–4] or $N_f = 2+1+1$ [5]. At higher temperatures, our understanding has relied almost exclusively on perturbative expansions in the strong coupling constant g . However, the convergence of the perturbative series is notoriously poor and at the order g^6 for the pressure [6], the expansion becomes sensitive to ultrasoft modes that are inherently non-perturbative. Previous studies in SU(3) Yang-Mills theory [7] and investigations of QCD screening masses [8, 9] indicate that perturbative predictions remain significantly far from the full result even at temperatures approaching the electroweak scale. This suggests that the smooth approach to the Stefan-Boltzmann limit may hide complex dynamics with non-perturbative contributions that can be resolved only through first-principles calculations.

In these proceedings, we present an overview of the strategy and the results of a fully non-perturbative computation of the QCD EoS across an unprecedented range of temperatures, from 3 GeV up to 165 GeV [10, 11]. We focus on the theory with $N_f = 3$ massless quarks, a choice justified by the negligible impact of the light quark masses at these energy scales. This progress relies on two key issues. First, the scale-setting problem is addressed through non-perturbative renormalization techniques in finite-volume schemes combined with step-scaling methods, which allowed us to define lines of constant physics by following the running of a renormalized coupling up to very high energies. Second, QCD is formulated in a moving reference frame through shifted boundary conditions in the Euclidean time direction [12–14]. This allows for a direct determination of the entropy density and eliminates the need for large ultraviolet subtractions of vacuum contributions.

The methodology discussed here is general and provides a framework that can be directly applied to QCD with four or five massive quark flavors.

2. Theoretical Framework

We consider Quantum Chromodynamics with $N_f = 3$ degenerate quark flavours regularized on a Euclidean lattice of size $L_0/a \times (L/a)^3$, where a is the lattice spacing. The action of the lattice theory $S_{QCD} = S_G + S_F$ is the sum of a pure gauge part, S_G , and a fermionic one, S_F . For the gauge sector we consider the Wilson plaquette action [15],

$$S_G = \frac{6}{g_0^2} \sum_x \sum_{\mu < \nu} \left[1 - \frac{1}{3} \text{Re tr} \{ U_{\mu\nu}(x) \} \right], \quad (1)$$

with g_0 being the bare coupling and $U_{\mu\nu}$ the plaquette field

$$U_{\mu\nu}(x) = U_\mu(x) U_\nu(x + a\hat{\mu}) U_\mu(x + a\hat{\nu})^\dagger U_\nu(x)^\dagger, \quad (2)$$

defined starting from the link field $U_\mu(x) \in \text{SU}(3)$. The fermionic action is

$$S_F = a^4 \sum_x \bar{\psi}(x) (D + M_0) \psi(x), \quad (3)$$

where the fermionic (antifermionic) fields ψ ($\bar{\psi}$) are triplets in color and flavour space and $M_0 = m_0 \mathbb{1}$ is the bare mass matrix of $N_f = 3$ degenerate quarks. The lattice Dirac operator is defined as

$$D = D_w + aD_{\text{sw}}, \quad (4)$$

where D_w is the massless Wilson-Dirac operator [16]

$$D_w = \frac{1}{2} \{ \gamma_\mu (\nabla_\mu^* + \nabla_\mu) - a \nabla_\mu^* \nabla_\mu \}, \quad (5)$$

and D_{sw} is the Sheikholeslami-Wohlert improvement term [17]

$$D_{\text{sw}} \psi(x) = c_{\text{sw}}(g_0) \frac{1}{4} \sigma_{\mu\nu} \widehat{F}_{\mu\nu}(x) \psi(x), \quad (6)$$

with $\sigma_{\mu\nu} = \frac{i}{2} [\gamma_\mu, \gamma_\nu]$. The coefficient $c_{\text{sw}}(g_0)$ is tuned non-perturbatively [18] to remove leading $\mathcal{O}(a)$ discretization effects [17, 19]. The covariant lattice derivatives act on the quark fields as

$$\begin{aligned} a \nabla_\mu \psi(x) &= U_\mu(x) \psi(x + a\hat{\mu}) - \psi(x), \\ a \nabla_\mu^* \psi(x) &= \psi(x) - U_\mu(x - a\hat{\mu})^\dagger \psi(x - a\hat{\mu}), \end{aligned} \quad (7)$$

while the lattice field strength tensor $\widehat{F}_{\mu\nu}(x)$ is defined by the clover discretization

$$\widehat{F}_{\mu\nu}(x) = \frac{i}{8a^2} \{ Q_{\mu\nu}(x) - Q_{\nu\mu}(x) \}, \quad (8)$$

with

$$\begin{aligned} Q_{\mu\nu}(x) &= U_\mu(x) U_\nu(x + a\hat{\mu}) U_\mu(x + a\hat{\nu})^\dagger U_\nu(x)^\dagger \\ &+ U_\nu(x) U_\mu(x - a\hat{\mu} + a\hat{\nu})^\dagger U_\nu(x - a\hat{\mu})^\dagger U_\mu(x - a\hat{\mu}) \\ &+ U_\mu(x - a\hat{\mu})^\dagger U_\nu(x - a\hat{\mu} - a\hat{\nu})^\dagger U_\mu(x - a\hat{\mu} - a\hat{\nu}) U_\nu(x - a\hat{\nu}) \\ &+ U_\nu(x - a\hat{\nu})^\dagger U_\mu(x - a\hat{\nu}) U_\nu(x + a\hat{\mu} - a\hat{\nu}) U_\mu(x)^\dagger. \end{aligned} \quad (9)$$

Periodic boundary conditions are imposed in the spatial directions for both the gauge and the fermion fields. In the temporal direction, we instead implement shifted boundary conditions [12–14]

$$\begin{aligned} U_\mu(x_0 + L_0, \mathbf{x}) &= U_\mu(x_0, \mathbf{x} - L_0 \boldsymbol{\xi}), \\ \psi(x_0 + L_0, \mathbf{x}) &= -\psi(x_0, \mathbf{x} - L_0 \boldsymbol{\xi}), \\ \bar{\psi}(x_0 + L_0, \mathbf{x}) &= -\bar{\psi}(x_0, \mathbf{x} - L_0 \boldsymbol{\xi}). \end{aligned} \quad (10)$$

The spatial vector $\boldsymbol{\xi}$ represents a constant shift that generalizes the standard thermal boundary conditions that are recovered for $\boldsymbol{\xi} = 0$. A non-vanishing shift corresponds to formulating the theory in a moving reference frame and plays a central role in the computation of thermodynamic observables. The partition function and thermal expectation values are defined by

$$\mathcal{Z}_\xi = \int DUD\bar{\psi}D\psi e^{-S_{QCD}}, \quad \langle O \rangle_\xi = \frac{1}{\mathcal{Z}_\xi} \int DUD\bar{\psi}D\psi O(U, \bar{\psi}, \psi) e^{-S_{QCD}}. \quad (11)$$

2.1 Lines of Constant Physics

A central challenge in high-temperature lattice simulations is the precise determination of the Lines of Constant Physics (LCPs). In order to extract results valid in the continuum limit from numerical simulations on the lattice, the bare parameters of the action must be tuned as the lattice spacing a is reduced, so that renormalized physical observables remain invariant up to discretization effects. This is typically achieved by fixing a set of hadronic observables.

At finite temperature, however, when T extends far beyond the hadronic scale M_{had} , such a strategy becomes impractical and computationally prohibitive. In fact, the lattice must simultaneously accommodate both the hadronic and the thermal scale, requiring it to be fine enough to resolve short distances while also large enough to capture long-range infrared dynamics. This leads to the hierarchy $L \gg M_{had}^{-1} \gg T^{-1} \gg a$ which requires exceedingly large volumes in lattice units. This *window problem* effectively prevents the use of usual hadronic renormalization schemes in the study of high-temperature thermodynamics.

To overcome this limitation, we adopt the strategy presented in Ref. [7, 8], in which the LCPs are defined through a renormalized coupling computed non-perturbatively in a finite volume. The non-perturbative running of renormalized couplings in the Schrödinger Functional (SF) and in the Gradient Flow schemes has been determined with high precision over a wide range of energy scales [20–23], as shown in Fig. 1 (taken from Ref. [24]). In particular, we consider the SF

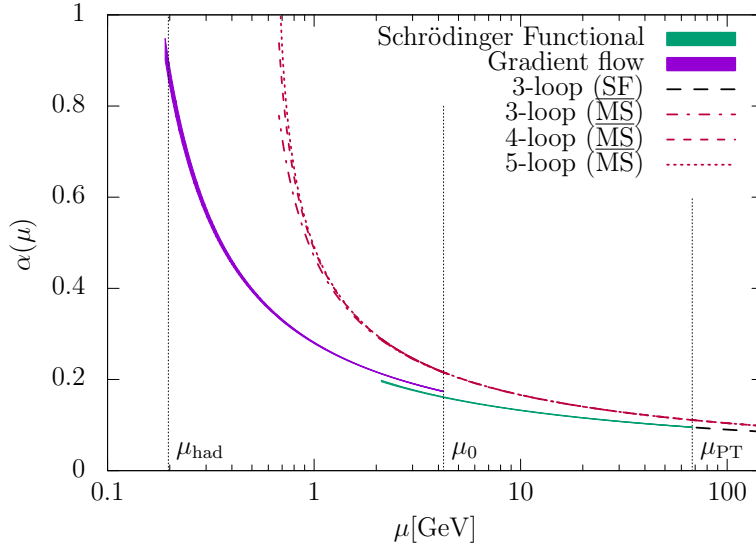


Figure 1: Non-perturbative running of renormalized gauge couplings for QCD with $N_f = 3$ over a wide range of momentum scales. Plot taken from Ref. [24].

scheme [25–27], where the renormalization scale μ is set by the inverse box size, and the LCPs are defined by fixing the value of the renormalized coupling at a reference scale $\mu = 1/L_0$ for different lattice spacings

$$\bar{g}_{\text{SF}}^2(g_0^2, a\mu) = \bar{g}_{\text{SF}}^2(\mu), \quad a\mu \ll 1. \quad (12)$$

This construction enables a controlled evolution from the hadronic to the electroweak scale through a sequence of finite-volume steps. In this framework, the bare parameters required for the high-temperature simulations are determined with high precision, as detailed in Ref. [8].

2.2 Thermodynamics from a moving frame

The standard approach to determining the EoS on the lattice is the *integral method* [28, 29]. In this framework, the pressure $p(T)$ is obtained by integrating the trace anomaly $\Theta(T) = e(T) - 3p(T)$ over a range of temperatures

$$\frac{p(T)}{T^4} = \frac{p(T_0)}{T_0^4} + \int_{T_0}^T \frac{\Theta(T')}{T'^5} dT' \quad (13)$$

where $e(T)$ is the energy density and T_0 is a reference temperature, typically chosen at low temperature where the pressure is assumed to be negligible. Although this method has been highly successful in lattice thermodynamics, the trace anomaly, being a dimension-four operator with a UV divergence $\propto a^{-4}$, requires subtracting a reference expectation value at the same lattice spacing. If the reference and the target temperatures are significantly separated, the subtraction involves two different energy scales, which can make the computation numerically demanding.

This limitation can be circumvented by formulating QCD in a moving reference frame. As discussed in Eq. (10), this corresponds to imposing shifted boundary conditions in the temporal direction with a non-vanishing spatial shift vector ξ . The key advantage of this geometric setup is that it enables a direct determination of the entropy density $s(T)$ without any temperature subtraction, so that simulations are performed only at the temperature of interest.

The entropy density is obtained from the dependence of the free-energy density on the shift parameter, studying the thermodynamic response of the system under variations of ξ . By exploiting the relativistic invariance of the theory, it can be shown [14] that the thermodynamics of the shifted system is equivalent to that of a static frame at a temperature determined by both the temporal extent L_0 and the shift vector ξ . Defining the geometric factor $\gamma = 1/\sqrt{1 + \xi^2}$, the inverse temperature is given by $T^{-1} = L_0/\gamma$. In the thermodynamic limit, the following relation holds between the free-energy densities computed in the moving and in the static frames

$$f_\xi(L_0) = - \lim_{L \rightarrow \infty} \frac{1}{L_0 L^3} \ln \mathcal{Z}_\xi(L_0, L, L, L) = - \lim_{L \rightarrow \infty} \frac{1}{L_0 L^3} \ln \mathcal{Z}_{\xi=0}(L_0/\gamma, L\gamma, L, L) = f_{\xi=0}(L_0/\gamma). \quad (14)$$

For simplicity, the shift vector is taken along one of the spatial directions. This identity reflects the underlying relativistic nature of the shifted boundary conditions: introducing a non-vanishing shift is equivalent to performing a Lorentz boost in Euclidean space. The geometric transformation has two simultaneous effects that the shift mixes: a time dilatation, where the effective temporal extent becomes $L'_0 = L_0/\gamma$ and a spatial contraction in the direction of the shift $L' = L\gamma$, such that the space-time volume element $L_0 V = L'_0 V'$ remains invariant.

By keeping L_0 and L fixed and varying the shift parameter, we can determine the entropy density through the expansion of the shift derivative

$$\frac{\partial}{\partial \xi_k} = \frac{\partial(1/T)}{\partial \xi_k} \frac{\partial}{\partial(1/T)} + \frac{\partial V'}{\partial \xi_k} \frac{\partial}{\partial V'}. \quad (15)$$

Using the thermodynamic identity $Ts(T) = e(T) + p(T)$, it follows that the derivative of the free energy density with respect to ξ_k leads to the following fundamental relation with the entropy density

$$\frac{s}{T^3} = \frac{1 + \xi^2}{\xi_k} \frac{1}{T^4} \frac{\partial f_\xi}{\partial \xi_k} \longrightarrow \frac{s}{T^3} = \frac{1 + \xi^2}{\xi_k} \frac{1}{T^4} \frac{\Delta f_\xi}{\Delta \xi_k}. \quad (16)$$

The expression on the right represents the lattice discretization of the derivative, which allows a non-perturbative computation of the entropy density through numerical simulations.

A fully non-perturbative determination of the entropy density can also be obtained from the expectation values of matrix elements of the renormalized energy-momentum tensor $T_{\mu\nu}$ on the lattice. In the lattice regularization, the explicit breaking of translational and rotational invariance implies that $T_{\mu\nu}$ is no longer protected by the usual continuum conservation laws and finite renormalization constants are required to recover the correct properties in the continuum limit. At present, these constants are known only at one-loop order in perturbation theory [30, 31] and a fully non-perturbative determination is still lacking.

3. Numerical computation

The entropy density is computed using Eq. (16) employing the two-point symmetric discretization for the derivative of the free-energy density with respect to the k -th component of the shift

$$\frac{\Delta f_\xi}{\Delta \xi_k} = \frac{L_0}{4a} \left(f_{\xi + \frac{2a}{L_0} k} - f_{\xi - \frac{2a}{L_0} k} \right). \quad (17)$$

From a computational perspective, it is advantageous to decompose the discrete derivative of the free-energy density into two separate contributions at fixed bare parameters

$$\frac{\Delta f_\xi}{\Delta \xi_k} = \frac{\Delta f_\xi^\infty}{\Delta \xi_k} + \frac{\Delta(f_\xi - f_\xi^\infty)}{\Delta \xi_k}, \quad (18)$$

where f_ξ^∞ denotes the free-energy density in the limit of infinitely heavy quarks, corresponding to the SU(3) pure gauge theory. The first term on the right-hand side is evaluated by rewriting it as an integral over the bare coupling g_0^2

$$\frac{\Delta f_\xi^\infty}{\Delta \xi_k} = \frac{\Delta f^{(0),\infty}}{\Delta \xi_k} + g_0^2 \frac{\Delta f^{(1),\infty}}{\Delta \xi_k} - \int_0^{g_0^2} du \left(\frac{1}{u} \frac{\Delta \langle \overline{S_G} \rangle_\xi^\infty}{\Delta \xi_k} \Big|_{g_0^2=u} + \frac{\Delta f^{(1),\infty}}{\Delta \xi_k} \right). \quad (19)$$

where $f^{(0),\infty}$ and $f^{(1),\infty}$ denote, respectively, the tree-level and the one-loop coefficients of the expansion in lattice perturbation theory of the pure gauge free-energy density [32]. The integral involves the expectation value of the SU(3) pure gauge action density in the moving reference frame

$$\langle \overline{S_G} \rangle_\xi^\infty = \frac{a^4}{L_0 L^3} \langle S_G \rangle_\xi^\infty. \quad (20)$$

and the subtraction of the one-loop coefficient has the purpose of ensuring a numerically more stable integration from the weak-coupling limit.

The second term in Eq. (18) accounts for the dynamic contribution of the three massless quark flavours. At fixed system size and bare gauge coupling, it can be determined by integrating the expectation value of the scalar density $\langle \overline{\psi} \psi \rangle_\xi^{m_q}$ – which represents the response of the system to variations in the quark mass – over a range connecting the chiral and the static limits

$$\frac{\Delta(f_\xi - f_\xi^\infty)}{\Delta \xi_k} = -\frac{\Delta}{\Delta \xi_k} \int_0^\infty dm_q \frac{\partial f_\xi^{m_q}}{\partial m_q} = -\int_0^\infty dm_q \frac{\Delta \langle \overline{\psi} \psi \rangle_\xi^{m_q}}{\Delta \xi_k}, \quad (21)$$

where $m_q = m_0 - m_{\text{cr}}(g_0^2, L_0)$ and m_{cr} is the critical mass.

The numerical evaluation of the entropy density thus relies on the lattice determination of the two above contributions and Monte Carlo simulations have been performed at the set of temperatures reported in Table 2, corresponding to fixed values of the Schrödinger Functional coupling at the scale $\mu = 1/L_0$. The shift vector entering the definition of the entropy density has been set to $\xi = (1, 0, 0)$. For each temperature, the spatial size has been fixed to $L/a = 144$ while four lattice resolutions in the temporal direction have been considered, $L_0/a = 4, 6, 8, 10$, corresponding to values for $(aT)^{-1}$ between 5.6 and 14. This choice ensures aspect ratios LT in the range ~ 10 –25, sufficiently large to suppress finite-volume effects.

3.1 Determination of $\frac{\Delta f_\xi^\infty}{\Delta \xi_k}$

The contribution of $\Delta f_\xi^\infty / \Delta \xi_k$ is obtained computing the integral over the bare coupling appearing in Eq. (19). The corresponding integrand is a smooth function of g_0^2 , allowing for an accurate numerical evaluation through a suitable combination of quadrature rules. The integration domain in g_0^2 is partitioned into intervals where different quadrature schemes are applied, including Simpson, trapezoidal and Gauss–Legendre rules. At fixed L_0/a , the computation proceeds recursively in the temperature: once the integral is determined up to a given value of the bare coupling, the result at lower temperatures is obtained by adding the contribution from the subsequent interval in g_0^2 . This strategy minimizes the number of independent integrations while maintaining high numerical accuracy. At each quadrature point, the expectation value of the gauge action density is computed in pure SU(3) Yang–Mills theory at the two values of the shift given in Eq. (17). The specifics of the integration scheme are detailed in Table 1. Gauge ensembles are generated using a combination of heat-bath and over-relaxation updates implemented via the Cabibbo–Marinari procedure. The statistical precision of this contribution depends on the lattice resolution. Coarser lattices achieve permille-level accuracy, while at the finest lattice spacing the uncertainty increases to the percent level, reflecting the higher computational cost. The integrand function of Eq. (19) is illustrated in Figure 2 for the four lattice resolutions $L_0/a = 4, 6, 8, 10$. The final results can be found in Table II in Ref. [10].

Interval	Quadrature	
$0 \leq g_0^2 \leq 6/15$	3 (Simpson)	$L_0/a = 4$
	2 (trapezoid)	$L_0/a = 6, 8, 10$
$6/15 \leq g_0^2 \leq 6/9$	3 (Gauss-Legendre)	
$6/9 \leq g_0^2 \leq g_0^2 T_0$	3 (Gauss-Legendre)	$L_0/a = 4$
	1 (midpoint)	$L_0/a = 6$
$6/9 \leq g_0^2 \leq g_0^2 T_1$	3 (Gauss-Legendre)	
$g_0^2 T_{i-1} \leq g_0^2 \leq g_0^2 T_i$	3 (Gauss-Legendre)	$1 < i < 7$
	5 (Gauss-Legendre)	$i = 7, 8$

Table 1: Summary of the integration scheme for the computation of the integral in g_0^2 appearing in Eq. (19).

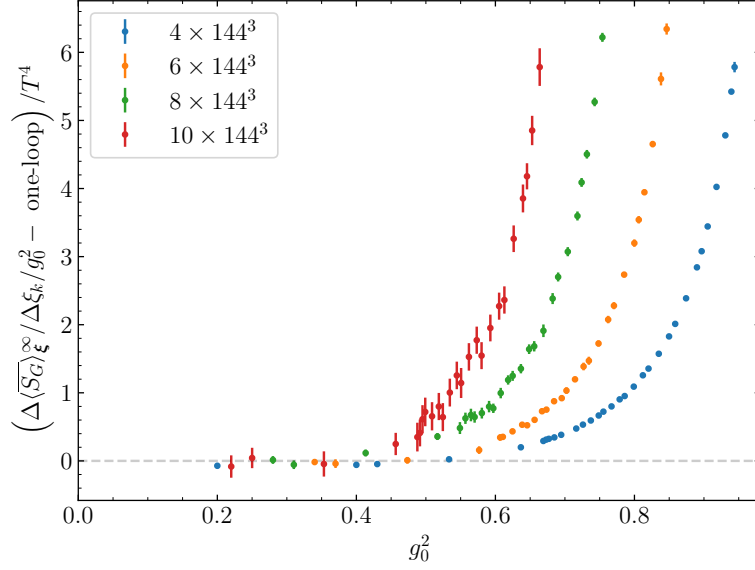


Figure 2: Plot of the integrand function in Eq. (19) as a function of the bare coupling g_0^2 . Points have been shifted horizontally by $0.03 \times (L_0/a - 4)$ for better readability.

3.2 Determination of $\frac{\Delta(f_\xi - f_\xi^\infty)}{\Delta\xi_k}$

The contribution of $\Delta(f_\xi - f_\xi^\infty)/\Delta\xi_k$ is evaluated from the integral over the bare subtracted quark mass in Eq. (21). The integration range is split into three regions in terms of the dimensionless variable $\tilde{m}_q = m_q/T$, allowing for an optimized representation of the integrand over the full mass range from the chiral to the static limit. Gaussian quadratures of different orders are employed in each region, ensuring that systematic effects from the numerical integration remain negligible compared to the statistical uncertainties. In the large-mass region, a change of variables to the hopping parameter makes the integration domain finite and improves numerical stability. The computation requires evaluating the scalar density expectation value at a set of quark masses corresponding to the quadrature nodes. For each lattice setup, simulations are performed at multiple mass values and for two shift vectors, resulting in a sizable number of independent ensembles.

A key optimization arises from the behaviour of the fermionic sector at large quark masses. As the quark mass increases, fermionic contributions become progressively suppressed, allowing a coarser integration of the molecular dynamics in the Hybrid Monte Carlo algorithm without degrading acceptance rates. This feature is exploited to significantly reduce computational costs. Moreover, a variance reduction in the heavy quark mass regime is achieved through introducing an improved estimator [33] of the chiral condensate obtained by subtracting the leading non-trivial order in the hopping parameter expansion.

Finally, the computational effort at the various quadrature points is optimized by taking into account both the variance of the observable and the weight of each node in the integration formula. This strategy ensures that the overall uncertainty is minimized for a fixed computational budget, yielding a significant gain in efficiency compared to collecting uniform statistics across all mass values. The non-perturbative integrand function is represented in Figure 3 for different values of the lattice spacing (left panel) and at different temperatures (right panel). Overall, the combination

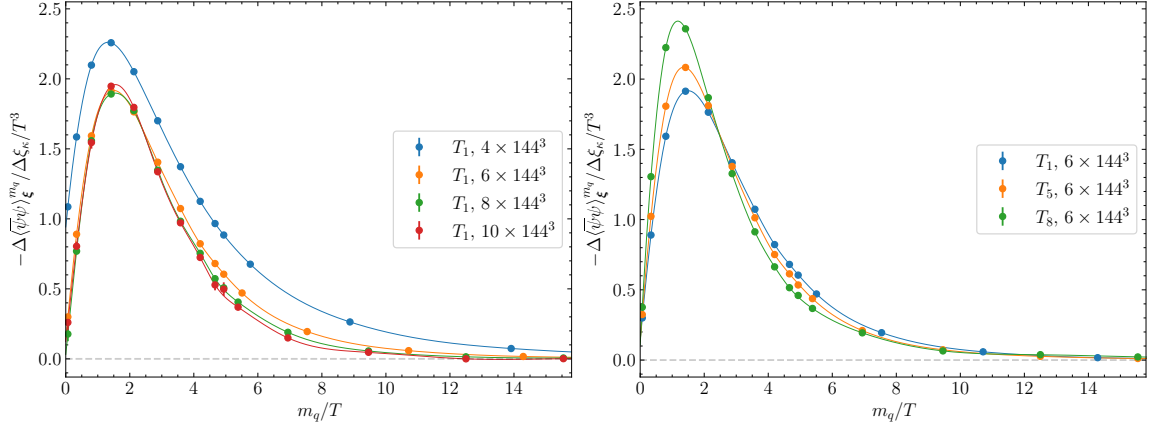


Figure 3: Left: plot of the integrand function in Eq. (21) computed at the bare parameters of temperature T_1 and at the resolutions $L_0/a = 4, 6, 8, 10$, as a function of m_q/T . Points have been interpolated with a cubic spline to guide the eye. In most cases, errors are smaller than the markers. Right: the same integrand function is shown at the resolution $L_0/a = 6$ and at three temperatures.

of optimized integration schemes, algorithmic improvements, and variance reduction techniques enables a precise determination of both contributions to the entropy density over the full range of temperatures and lattice spacings considered. The final results can be found in Table II in Ref. [10].

3.3 Extrapolation to the continuum limit

The final results for the discrete derivative of the free energy density with respect to the shift can be found in Table III in Ref. [11] and the continuum limit is obtained after implementing a one-loop perturbative improvement that removes lattice artifacts at tree-level and at $O(g^2)$. The remaining cutoff effects are therefore suppressed and expected to start at $O(a^2g^3)$, consistently with $O(a)$ -improvement and the presence of odd powers in the coupling at finite temperature. The extrapolation is performed with a global fit of the data at all temperatures, in which discretization effects are modeled as polynomials in \bar{g}_{SF} . A careful analysis of fit stability shows that the coarsest lattice $L_0/a = 4$ is significantly affected by higher-order discretization artifacts. It is therefore excluded from the preferred fit but its impact is taken into account to estimate the systematic uncertainty associated to higher-order corrections in the lattice spacing. The final estimate uses data at $L_0/a = 6, 8$ and 10 and a minimal ansatz for cutoff effects, yielding continuum values with sub-percent precision. Several variations of the fit ansatz, including higher-order terms in a and in the coupling, as well as logarithmic corrections, lead to results fully compatible within uncertainties, showing that the continuum extrapolation is robust and that residual discretization effects are well under control. The final continuum results for the entropy density are reported in Table 2 and have a relative error of 0.5-1.0% and Figure 4 displays the related continuum limit extrapolations.

Finite-volume effects in high-temperature lattice simulations are exponentially suppressed as $e^{-M_{\text{gap}}L}$, where M_{gap} is the mass of the lightest screening state. In the temperature regime investigated here, the screening mass is approximately of the order of the physical temperature T . Given that the simulations were performed on lattices with aspect ratios ranging between $10 \lesssim LT \lesssim 25$, finite-size corrections are expected to be negligible compared to the statistical precision of our

T	T (GeV)	$\bar{g}_{\text{SF}}^2(\mu = 1/L_0)$	s/T^3
T_0	164.6(5.6)	1.01636	20.13(8)
T_1	82.3(2.8)	1.11000	20.05(8)
T_2	51.4(1.7)	1.18446	20.05(9)
T_3	32.8(1.0)	1.26569	19.90(9)
T_4	20.63(63)	1.3627	19.93(10)
T_5	12.77(37)	1.4808	19.87(11)
T_6	8.03(22)	1.6173	19.75(12)
T_7	4.91(13)	1.7943	19.74(15)
T_8	3.040(78)	2.0120	19.58(17)

Table 2: Second column: physical temperatures considered in this study. Third column: values of the Schrödinger functional coupling in $N_f = 3$ QCD at the renormalization scale $\mu = 1/L_0$. Fourth column: values of the entropy density in the continuum limit.

results. This expectation was explicitly validated through dedicated simulations at varying spatial volumes, which showed no statistically significant deviations in the thermodynamic observables.

Concerning the topological sampling, the dominance of the trivial sector at high temperatures justifies restricting the measurements accordingly. While occasional tunneling between topological sectors was observed at the lowest temperatures and coarsest lattice spacings in the pure gauge simulations, no statistically significant dependence of the action density on the topological charge was detected. Nevertheless, to account for potential residual effects in the expectation value of the action density due to limited topological sampling, a conservative systematic uncertainty of up to 2% has been included in the error estimates of $\Delta\langle S_G \rangle_{\xi}^{\infty}$ for those cases.

4. Equation of State

The data generated by the Monte Carlo simulations and the extrapolation of the results to the continuum limit allowed to investigate the temperature dependence of the thermodynamic potentials over the broad range of temperatures between 3 GeV and 165 GeV [10, 11]. For convenience, we express the results in terms of $\hat{g}(\mu)$ defined as the five-loop $\overline{\text{MS}}$ coupling [34] at the renormalization scale $\mu = 2\pi T$, whose leading order expression is

$$\frac{1}{\hat{g}^2(\mu)} = \frac{9}{8\pi^2} \ln \frac{\mu}{\Lambda_{\overline{\text{MS}}}} + \dots, \quad \mu = 2\pi T, \quad (22)$$

where $\Lambda_{\overline{\text{MS}}} = 341$ MeV is taken from Ref. [24]. For our purposes, this is only a convenient function of T for studying the temperature dependence of the non-perturbative results and which, at the same time, simplifies the comparison with the perturbative expectations.

The continuum-extrapolated results for the entropy density have a remarkably smooth dependence on \hat{g}^2 suggesting that it may be an effective variable for characterizing the thermal behaviour of the theory in the high-temperature regime. In order to describe the data and to facilitate the comparison with perturbation theory, we parametrize the entropy density using a polynomial expansion

$$\frac{s}{T^3} = \frac{32\pi^2}{45} \sum_k s_k \left(\frac{\hat{g}}{2\pi} \right)^k. \quad (23)$$

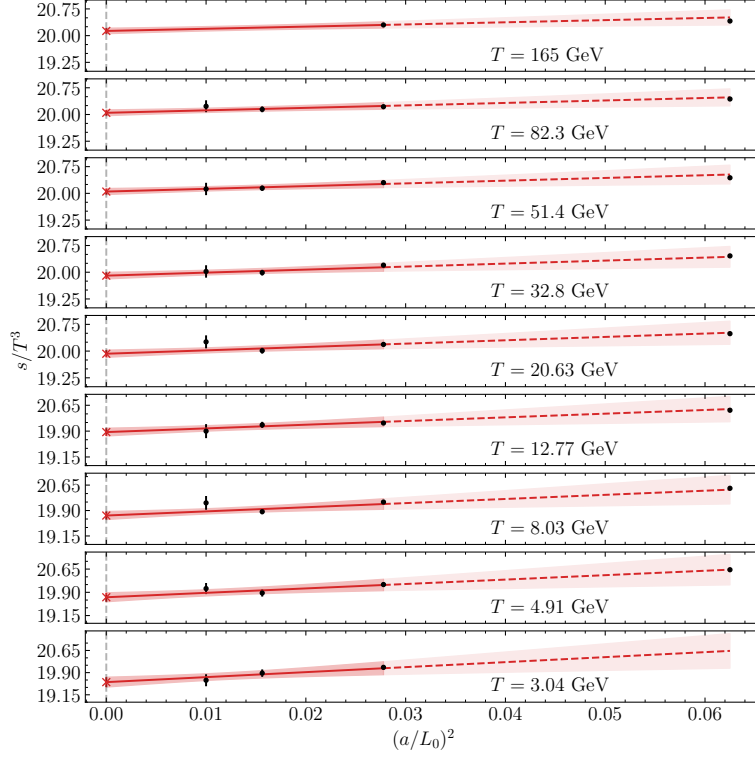


Figure 4: Black dots are the values of the one-loop improved entropy density as a function of $(a/L_0)^2$ at the temperatures T_0, T_1, \dots, T_8 . The red band is our best extrapolation to the continuum limit and red crosses are the continuum extrapolated values for s/T^3 . The horizontal axis is common to all the subplots.

Several fit strategies have been explored in order to assess systematic uncertainties and the sensitivity to the asymptotic behaviour at high temperature. We can enforce the Stefan–Boltzmann limit (SB) at asymptotically large T fixing the leading coefficient to the ideal gas value $s_0 = s_0^{\text{SB}} = 2.969$ (for $N_f = 3$) and leaving the first two non-trivial coefficients as fit parameters. As shown in Fig. 5, this parametrization provides an excellent description of the data across the investigated temperature range and the estimated values of the parameters are $s_2 = -5.1(9)$ and $s_3 = 5(5)$. While the quality of the fit is high, a first comparison with perturbation theory shows a significant deviation with respect to the expected value of the quadratic coefficient $s_2 = -8.438$.

We have then compared – see Fig. 6 – the non-perturbative results for s/T^3 with the perturbative predictions of high-temperature QCD, computed both in standard perturbation theory and in hard thermal loop (HTL) resummed approaches, respectively known up to $O(g^6 \ln g^2)$ and to NNLO. In conventional perturbation theory, the expansion exhibits poor convergence in the considered temperature range. Successive orders show significant deviations, indicating that higher-order contributions are relevant even at temperatures as high as $T \sim 100$ GeV. HTL-resummed calculations improve the apparent convergence, especially at the highest temperatures, but still display visible tensions between successive orders. The comparison with the non-perturbative data shows that even the most accurate HTL results do not fully capture the dynamics in the explored regime.

As alternative fit strategy we have incorporated all known perturbative coefficients, fitting only the unknown higher-order terms. It is important to note that at $O(g^6)$ non-perturbative contributions

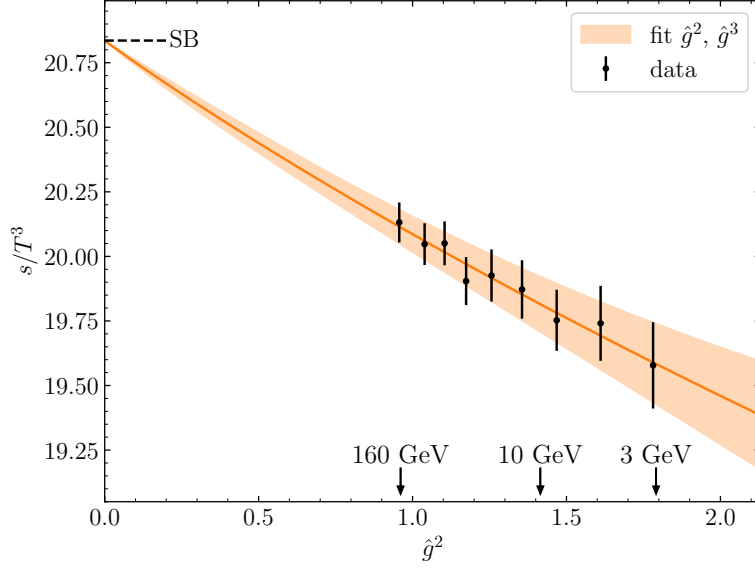


Figure 5: Temperature dependence of the entropy density in terms of \hat{g}^2 . The data are fitted by enforcing the Stefan–Boltzmann limit (SB) at infinite temperature and including quadratic and cubic corrections. The shaded area indicates the uncertainty of the fit.

to the pressure appear that cannot be computed in the framework of perturbation theory [6]. Our preferred parametrization of the non-perturbative data involves \hat{g}^6 and \hat{g}^7 terms and includes the entropy density at $T = 500$ MeV obtained from independent lattice calculations with $N_f = 2 + 1$ flavours [2–4]. This input effectively constrains the interpolation at lower temperatures and leads to a global description of the entropy density valid for $T \geq 500$ MeV. This phenomenological fit is shown in the left panel of Fig. 7.

Using this parametrization of the entropy density, the pressure and energy density can be obtained consistently. Analogously to Eq. (23), we parametrize the pressure as a polynomial expansion and its coefficients are directly related to those of the entropy density through the thermodynamic identity $s(T) = \frac{d}{dT} p(T)$. The energy density is then obtained from $e(T) = Ts(T) - p(T)$. As a cross-check, we have computed the pressure by integrating the entropy density starting from $T_0 = 500$ MeV and $p(T_0)/T_0^4 = 4.050(38)$ taken from independent lattice determinations [2–4]. The two procedures yield fully compatible results across the entire temperature range, providing a non-trivial validation of the consistency of the analysis. The temperature dependence of the thermodynamic potentials is shown in the right panel of Fig. 7.

5. Conclusions and Outlook

The results presented in these proceedings show that current theoretical and computational advances in lattice QCD permit a fully non-perturbative investigation of QCD thermodynamics up to the electroweak scale. The QCD Equation of State for $N_f = 3$ massless quarks has been computed with a precision of 0.5-1% across the previously unexplored temperature range between 3 GeV and 165 GeV [10, 11].

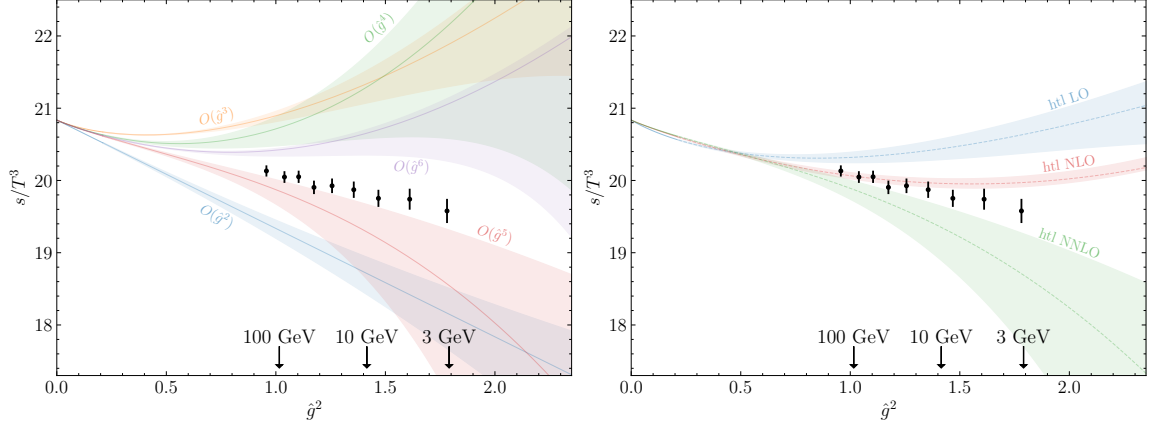


Figure 6: Black dots are the non-perturbative values of s/T^3 plotted against \hat{g}^2 . Some values of the physical temperature are reported for reference. In the left plot, the curves represent the predictions of perturbation theory obtained from Ref. [6], each including up to the order in \hat{g} indicated by the label. In the right plot, the curves represent the hard thermal loop perturbation theory [35–37] at leading order (LO), next-to-leading order (NLO) and next-to-next-to leading order (NNLO). In both plots, error bands are obtained by a variation of the renormalization scale $\mu = 2\pi T$ by the factors 0.5 and 2.

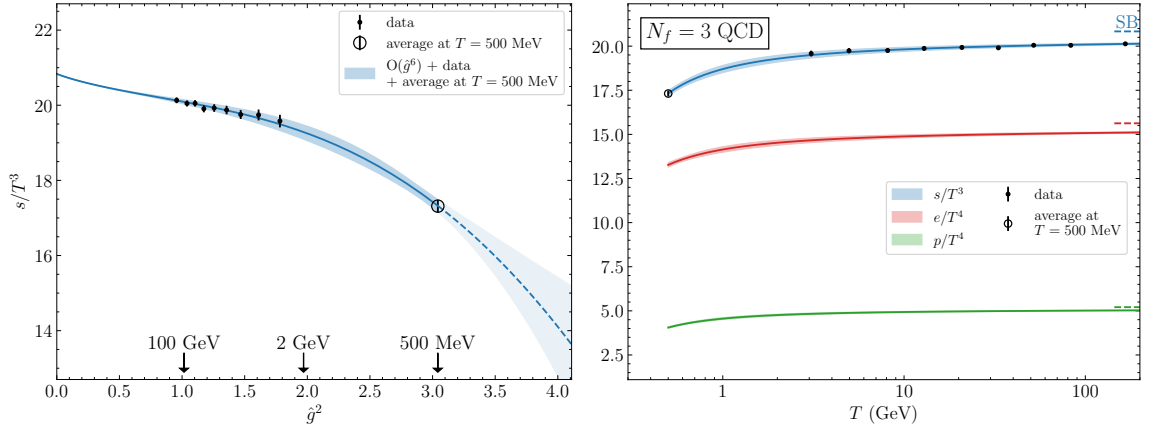


Figure 7: Left: entropy density s/T^3 in the continuum limit as a function of \hat{g}^2 . The blue band is the best parametrization for $T \geq 500$ MeV, and includes the point at $T = 500$ MeV obtained from Refs. [2–4] (open circle marker). Right: EoS as a function of the temperature for $T \geq 500$ MeV.

An important issue of this study is the behaviour of the entropy density as it approaches the Stefan–Boltzmann limit. While s/T^3 exhibits a relatively mild and smooth decrease from the ideal gas limit down to temperatures of a few GeV, this regularity should not be (mis)taken for an indication that the system is in a perturbative regime. In fact, our analysis shows that terms beyond the known $O(g^6)$ perturbative expansion that include non-perturbative contributions are necessary to describe the lattice data accurately up to the electroweak scale. Interestingly, we find that a phenomenological fit based on these extensions remains robust even down to $T \sim 500$ MeV.

The strategy developed for this study, combining shifted boundary conditions with the non-

perturbative running of the Schrödinger Functional coupling, represents an efficient approach that can be applied to include the cases of $N_f = 4$ and 5 massive flavours without further theoretical development, providing a clear path toward a complete description of the Standard Model's thermodynamic evolution in the early Universe.

Looking ahead, simulations are currently in progress to determine the non-perturbative renormalization constants of the energy-momentum tensor. They are essential for the calculation of transport coefficients whose accurate determination will be important for understanding the hydrodynamical features of the quark-gluon plasma in both heavy-ion collisions and cosmological contexts.

Acknowledgements. The results reported here were obtained with M. Bresciani, M. Dalla Brida, and L. Giusti, whom I gratefully acknowledge for their collaboration and for a critical reading of these proceedings. I also thank CINECA for providing us with a very generous access to Leonardo during the early phases of operations of the machine and for the computer time allocated via the CINECA-INFN, CINECA-Bicocca agreements. The R&D has been carried out on the PC clusters Wilson and Knuth at Milano-Bicocca. We thank all these institutions for the technical support. This work is (partially) supported by ICSC – Centro Nazionale di Ricerca in High Performance Computing, Big Data and Quantum Computing, funded by European Union – NextGenerationEU.

References

- [1] K. Saikawa and S. Shirai, *Primordial gravitational waves, precisely: The role of thermodynamics in the Standard Model*, *JCAP* **05** (2018) 035 [[1803.01038](#)].
- [2] S. Borsanyi, Z. Fodor, C. Hoelbling, S.D. Katz, S. Krieg and K.K. Szabo, *Full result for the QCD equation of state with 2+1 flavors*, *Phys. Lett. B* **730** (2014) 99 [[1309.5258](#)].
- [3] HotQCD collaboration, *Equation of state in (2+1)-flavor QCD*, *Phys. Rev. D* **90** (2014) 094503 [[1407.6387](#)].
- [4] A. Bazavov, P. Petreczky and J.H. Weber, *Equation of State in 2+1 Flavor QCD at High Temperatures*, *Phys. Rev. D* **97** (2018) 014510 [[1710.05024](#)].
- [5] S. Borsanyi et al., *Calculation of the axion mass based on high-temperature lattice quantum chromodynamics*, *Nature* **539** (2016) 69 [[1606.07494](#)].
- [6] K. Kajantie, M. Laine, K. Rummukainen and Y. Schroder, *The Pressure of hot QCD up to $g_6 \ln(1/g)$* , *Phys. Rev. D* **67** (2003) 105008 [[hep-ph/0211321](#)].
- [7] L. Giusti and M. Pepe, *Equation of state of the SU(3) Yang–Mills theory: A precise determination from a moving frame*, *Phys. Lett.* **B769** (2017) 385 [[1612.00265](#)].
- [8] M. Dalla Brida, L. Giusti, T. Harris, D. Laudicina and M. Pepe, *Non-perturbative thermal QCD at all temperatures: the case of mesonic screening masses*, *JHEP* **04** (2022) 034 [[2112.05427](#)].

- [9] L. Giusti, T. Harris, D. Laudicina, M. Pepe and P. Rescigno, *Baryonic screening masses in QCD at high temperature*, *Phys. Lett. B* **855** (2024) 138799 [2405.04182].
- [10] M. Bresciani, M. Dalla Brida, L. Giusti and M. Pepe, *QCD Equation of State with $N_f=3$ Flavors up to the Electroweak Scale*, *Phys. Rev. Lett.* **134** (2025) 201904 [2501.11603].
- [11] M. Bresciani, M. Dalla Brida, L. Giusti and M. Pepe, *QCD equation of state at very high temperature: Computational strategy, simulations, and data analysis*, *Phys. Rev. D* **113** (2026) 034506 [2511.09160].
- [12] L. Giusti and H.B. Meyer, *Thermal momentum distribution from path integrals with shifted boundary conditions*, *Phys. Rev. Lett.* **106** (2011) 131601 [1011.2727].
- [13] L. Giusti and H.B. Meyer, *Thermodynamic potentials from shifted boundary conditions: the scalar-field theory case*, *JHEP* **11** (2011) 087 [1110.3136].
- [14] L. Giusti and H.B. Meyer, *Implications of Poincare symmetry for thermal field theories in finite-volume*, *JHEP* **01** (2013) 140 [1211.6669].
- [15] K.G. Wilson, *Confinement of Quarks*, *Phys. Rev. D* **10** (1974) 2445.
- [16] K.G. Wilson, *Quarks: From Paradox to Myth*, *Subnucl. Ser.* **13** (1977) 13.
- [17] B. Sheikholeslami and R. Wohlert, *Improved Continuum Limit Lattice Action for QCD with Wilson Fermions*, *Nucl. Phys.* **B259** (1985) 572.
- [18] JLQCD, CP-PACS collaboration, *Non-perturbative $O(a)$ -improvement of Wilson quark action in three-flavor QCD with plaquette gauge action*, *Phys. Rev.* **D71** (2005) 054505 [hep-lat/0406028].
- [19] M. Lüscher, S. Sint, R. Sommer and P. Weisz, *Chiral symmetry and $O(a)$ improvement in lattice QCD*, *Nucl. Phys.* **B478** (1996) 365 [hep-lat/9605038].
- [20] M. Lüscher, R. Sommer, P. Weisz and U. Wolff, *A precise determination of the running coupling in the $SU(3)$ Yang-Mills theory*, *Nucl. Phys.* **B413** (1994) 481 [hep-lat/9309005].
- [21] ALPHA collaboration, *Determination of the QCD Λ -parameter and the accuracy of perturbation theory at high energies*, *Phys. Rev. Lett.* **117** (2016) 182001 [1604.06193].
- [22] ALPHA collaboration, *Slow running of the Gradient Flow coupling from 200 MeV to 4 GeV in $N_f = 3$ QCD*, *Phys. Rev. D* **95** (2017) 014507 [1607.06423].
- [23] ALPHA collaboration, *A non-perturbative exploration of the high energy regime in $N_f = 3$ QCD*, *Eur. Phys. J. C* **78** (2018) 372 [1803.10230].
- [24] ALPHA collaboration, *QCD Coupling from a Nonperturbative Determination of the Three-Flavor Λ Parameter*, *Phys. Rev. Lett.* **119** (2017) 102001 [1706.03821].

- [25] M. Lüscher, R. Narayanan, P. Weisz and U. Wolff, *The Schrödinger functional: a renormalizable probe for non-Abelian gauge theories*, *Nucl. Phys.* **B384** (1992) 168 [[hep-lat/9207009](#)].
- [26] S. Sint, *On the Schrödinger functional in QCD*, *Nucl. Phys.* **B421** (1994) 135 [[hep-lat/9312079](#)].
- [27] S. Sint and R. Sommer, *The running coupling from the QCD Schrödinger functional: a one-loop analysis*, *Nucl. Phys.* **B465** (1996) 71 [[hep-lat/9508012](#)].
- [28] G. Boyd, J. Engels, F. Karsch, E. Laermann, C. Legeland, M. Lutgemeier et al., *Equation of state for the SU(3) gauge theory*, *Phys. Rev. Lett.* **75** (1995) 4169 [[hep-lat/9506025](#)].
- [29] G. Boyd, J. Engels, F. Karsch, E. Laermann, C. Legeland, M. Lutgemeier et al., *Thermodynamics of SU(3) lattice gauge theory*, *Nucl. Phys. B* **469** (1996) 419 [[hep-lat/9602007](#)].
- [30] S. Caracciolo, P. Menotti and A. Pelissetto, *Analytic determination at one loop of the energy momentum tensor for lattice QCD*, *Phys. Lett.* **B260** (1991) 401.
- [31] S. Caracciolo, P. Menotti and A. Pelissetto, *One loop analytic computation of the energy momentum tensor for lattice gauge theories*, *Nucl. Phys.* **B375** (1992) 195.
- [32] M. Dalla Brida, L. Giusti and M. Pepe, *Non-perturbative definition of the QCD energy-momentum tensor on the lattice*, *JHEP* **04** (2020) 043 [[2002.06897](#)].
- [33] L. Giusti, T. Harris, A. Nada and S. Schaefer, *Frequency-splitting estimators of single-propagator traces*, *Eur. Phys. J. C* **79** (2019) 586 [[1903.10447](#)].
- [34] P.A. Baikov, K.G. Chetyrkin and J.H. Kühn, *Five-Loop Running of the QCD coupling constant*, *Phys. Rev. Lett.* **118** (2017) 082002 [[1606.08659](#)].
- [35] J.O. Andersen, E. Petitgirard and M. Strickland, *Two loop HTL thermodynamics with quarks*, *Phys. Rev. D* **70** (2004) 045001 [[hep-ph/0302069](#)].
- [36] J.O. Andersen, M. Strickland and N. Su, *Three-loop HTL gluon thermodynamics at intermediate coupling*, *JHEP* **08** (2010) 113 [[1005.1603](#)].
- [37] J.O. Andersen, L.E. Leganger, M. Strickland and N. Su, *Three-loop HTL QCD thermodynamics*, *JHEP* **08** (2011) 053 [[1103.2528](#)].